Radiation Awareness for Endovascular Abdominal Aortic Aneurysm Repair in the Hybrid Operating Room. An Instant Patient Risk Chart for Daily Practice

Quirina M. de Ruiter, MSc, PhD[1], Crystel M. Gijsberts, MD, PhD[2,3], Constantijn E. Hazenberg, MD, PhD[1], Frans L. Moll, MD, PhD[1], and Joost A. van Herwaarden, MD, PhD[1]

Abstract

Purpose: To determine which patient and C-arm characteristics are the strongest predictors of intraoperative patient radiation dose rates (DRs) during endovascular aneurysm repair (EVAR) procedures and create a patient risk chart. **Methods:** A retrospective analysis was performed of 74 EVAR procedures, including 16,889 X-ray runs using fixed C-arm imaging equipment. Four multivariate log-linear mixed models (with patient as a random effect) were constructed. Mean air kerma DR (DR_{AK}, mGy/s) and the mean dose area product DR (DR_{DAP}, mGycm^2/s) were the outcome variables utilized for fluoroscopy as differentiated from digital subtraction angiography (DSA). These models were used to predict the maximum radiation duration allowed before a 2-Gy skin threshold (for DR_{AK}) or a 500-Gycm^2 threshold (for DR_{DAP}) was reached. **Results:** The strongest predictor of DR_{AK} and DR_{DAP} for fluoroscopy imaging was the radiation protocol, with an increase of 200% when changing from "low" to "medium" and 410% from "low" to "normal." The strongest predictors of DR_{AK} and DR_{DAP} for DSA were C-arm angulation, with an increase of 47% per 30° of angulation, and body mass index (BMI), with an increase of 58% for every 5-point increase in BMI. Based on these models, a patient with a BMI of 30 kg/m^2, combined with 45° of rotation and a field size of 800 cm^2 in the medium fluoroscopy protocol has a predicted DR_{AK} of 0.39 mGy/s (or 85.5 minutes until the 2-Gy skin threshold is reached). While using comparable settings but switching the acquisition to a DSA with a "2 frames per second" protocol, the predicted DR_{AK} will be 6.6 mGy/s (or 5.0 minutes until the 2-Gy threshold is reached). **Conclusion:** X-ray radiation DRs are constantly fluctuating during and between patients based on BMI, the protocols, C-arm position, and the image acquisitions that are used. An instant patient risk chart visualizes these radiation dose fluctuations and provides an overview of the expected duration of X-ray radiation, which can be used to predict when follow-up dose thresholds are reached during abdominal endovascular procedures.

Keywords

abdominal aortic aneurysm, air kerma, C-arm image intensifier, digital subtraction angiography, dose area product, dose reduction, endovascular aneurysm repair, fluoroscopy, imaging technology, radiation dose, risk assessment, X-ray

Introduction

Fixed C-arm angiographic imaging systems in interventional or hybrid operating suites allow optimal guidance of endovascular aneurysm repair (EVAR) due to advanced 3-dimensional (3D) imaging techniques, high image quality, improved safety and efficiency, and the availability of high-contrast images.[1,2] Unfortunately, because improved image quality with a low signal-to-noise ratio correlates with radiation dose levels, these high-contrast X-ray images from fixed C-arms increase the radiation dose rates (DRs).[3]

Research on radiation exposure during EVAR primarily focuses on anthropomorphic phantoms using standardized protocols, which do not allow adjustments for individual patient characteristics or variations in the clinical setting.[4] Moreover, clinical studies usually present only the cumulative radiation dose per intervention.[5] Although these cumulative dose outcomes are interesting for comparing the mean doses between interventions or treatments or calculating the overall patient risk, they do not correct for the C-arm or patient characteristics. A gap in current research exists

describing which factors are the strongest predictors in determining the actual DRs in authentic clinical settings.

Taking into consideration that the final DR is multifactorial and analyzing these DR predictors should encompass a variety of patients and incorporate various DR predictors, such as the radiation protocol, body mass index (BMI), C-arm rotation and angulation, the air gap, and the field size. A multifactorial approach leads to a better understanding of the actual clinical DRs of each specific C-arm configuration and protocol, increases the operator's insight into the real-time DRs, improves radiation awareness, and can steer decision making for DR reduction during the intervention.

Employing 4 multivariable log-linear mixed models, this study examined the strength of each of the predictors on 2 DR outcome measures, air kerma (AK) and dose area product (DAP), for fluoroscopy as well as DSA during EVAR. The results from these models were used to predict the maximum radiation duration until reaching the 2-Gy (reference) skin threshold for AK or the 500-Gycm^2 for DAP.

Methods

Study Design

Since December 2013, a patient's cumulative radiation DR outcomes and C-arm settings for each X-ray run acquired during the intervention in our hybrid OR have been systematically reported in a Digital Imaging and Communications in Medicine–structured reporting (DICOM SR) format and filed in the hospital patient information system. These DICOM SR reports were examined for 74 consecutive patients (mean age 75.8±8.7 years; 55 men) who underwent an elective EVAR performed by a team of endovascular surgeons between December 2013 and January 2015. All intraoperative imaging was performed with the patient on a radiopaque carbon fiber Magnus table (Maquet Medical Systems, Wayne, NJ, USA) using a single-plane Allura FD20 angiographic C-arm system (Philips Healthcare, Best, the Netherlands) updated with AlluraClarity and ClarityIQ radiation-reduction technology. All operators had a minimum of 3 years' experience in endovascular procedures. Patient age, sex, BMI, and intervention details were extracted into a separate database; the patient characteristics are summarized in Table 1.

Table 1. Characteristics of the 74 Patients in the Study.[a]

Age, y	75.8±8.7
BMI, kg/m^2	26.3±3.7
Men	55 (74.3)
Intervention	
Aortouni-iliac graft	3 (4.1)
EVAR+ chimney	5 (6.8)
EVAR	41 (55.4)
EVAR+ IBD	8 (10.8)
FEVAR	17 (23.0)

Abbreviations: EVAR, endovascular aneurysm repair; FEVAR, fenestrated EVAR; IBD, iliac branch device.
[a]Continuous data are presented as the means ± standard deviation; categorical data are given as the counts (percentage).

Dose Metrics

AK is the strength of the beam exposure at 15 cm from the isocenter of the X-ray beam between the detector and the X-ray source. AK, calculated by the C-arm equipment, reflects the patient's skin dose and is also an indirect metric of the actual deterministic patient risk. AK is not corrected for dose distribution across the skin as a result of table movements, C-arm rotation or angulation, or field size. DAP, however, is an indirect stochastic parameter because it represents the total cumulative dose exposure as a product of beam strength (Gy or mGy) and field size (cm^2). DAP is measured with a meter built into the beam source of the equipment. The mean AK DR per X-ray run is referred to as DR_{AK} and is measured in mGy/s. The mean DAP DR per X-ray run is referred to as DR_{DAP} and is calculated in mGycm^2/s.

Imaging Protocols

On the basis of the C-arm settings, each X-ray run was categorized as a fluoroscopy run or a DSA run. The AlluraClarity C-arm has 3 fluoroscopy protocols with different dose levels, image contrast, and image density; they are labeled by the system as "low," "medium," and "normal" according to 3 levels of increasing image quality. With DSA, the 2 main protocols feature acquisition at 2 frames per second (fps) or at 3 fps. In our center, the 2-fps protocol is the standard protocol for vessel landmarking and the

[1]Department of Vascular Surgery, University Medical Center Utrecht, the Netherlands
[2]ICIN–Netherlands Heart Institute, Utrecht, the Netherlands
[3]Laboratory of Experimental Cardiology, University Medical Center Utrecht, the Netherlands

Corresponding Author:
Joost van Herwaarden, Department of Vascular Surgery, University Medical Center Utrecht, Heidelberglaan 100, Postbus 85500, 3508GA Utrecht, the Netherlands.
Email: j.a.vanherwaarden@umcutrecht.nl

Table 2. Primary Settings for Each Fluoroscopy and Digital Subtraction Angiography (DSA) Protocol.

	Fluoroscopy Protocol (15 fps)			DSA Protocol	
	Low	Medium	Normal	2 fps (>1–2)	3 fps (>2–3)
kV (min-max)	62–120	72–120	62–120	80–125	80–125
mA (min-max)	21–95	86–160	12–160	131–511	158–449
Pulse width	4–4.2	4–5.8	4–7.6	45–220	45–220
EDL, R/min	1.2	3	7	—	—
Filter, mm	0.4	0.4	0.1	0.1	0.1

Abbreviations: EDL, entrance dose limitation; fps, frames per second.

3-fps protocol is used for the final angiogram to check for vessel/device patency, existence of endoleaks, and outflow. Table 2 and Figure 1 summarize the baseline setup characteristics predefined by the manufacturer, including voltage and maximum dose thresholds.

Recorded C-arm Characteristics

Characteristics of each of the 18,811 X-ray runs in the patient cohort were extracted from the DICOM SR reports using Matlab 2015a software (Mathworks, Natick, MA, USA):

1. The cumulative radiation dose parameters: DAP_{run}, AK_{run}, the cumulative number of frames per run (Fr_{run}), and the total radiation (fluoroscopy) duration per run (FT_{run}, seconds).
2. The fixed imaging acquisition parameters per run: X-ray tube peak voltage, X-ray tube current, and X-ray copper spectral filter thickness.
3. The type of X-ray runs: fluoroscopy or stationary acquisition (ie, exposure images using DSA or single shots).
4. C-arm characteristics: fluoroscopy protocol, DSA protocol, the primary angle (rotation), secondary angle (angulation), source-to-image distance (SID) to calculate the air gap, and shutter locations from which field size can be calculated.

Statistical Analyses

As part of the exploratory data analysis, each independent variable was individually studied in a univariate analysis. The associations among C-arm characteristics, BMI, and the DR were examined with 4 multivariable log-linear mixed-effects regression models for fluoroscopy, DSA, DR_{AK}, and DR_{DAP}. Fixed effects were BMI, all available C-arm characteristics, protocol, rotation, angulation, field size, and air gap. A random intercept for the patient was added to account for patient-level clustering. The models, with and without random intercept, were compared using the goodness of fit, likelihood ratio, or Akaike information criterion. The residual plots were visually checked for obvious deviations from homoscedasticity or normality. Multicolinearity was assessed by evaluating the variance inflation factor; outliers in each model were checked on finding a pattern. P values were obtained by likelihood ratio tests of the full model with the predictor in question against the model without the predictor in question. The coefficient of multiple determination (R^2), intraclass correlation (ICC), and variance parameters for the random effects (σ^2) were obtained for each final model. The threshold of statistical significance was p<0.05.

Although BMI is a clinically relevant parameter of body size, body thickness may be a better predictor of radiation dose increases. Thus, BMI and body thicknesses manually measured on the preoperative computed tomography (CT) scans at the level of the renal arteries in anteroposterior (AP) and lateral views were tested for correlation. If there was a significant linear correlation, body thickness was replaced with BMI in further analyses.

Beta estimates and bootstrapped 95% confidence intervals (CI) were extracted from both univariate and multivariate models and back transformed to a nonlogarithmic scale presented as odds ratios (OR). An OR of ≤1 indicates no influence on the radiation dose, while an OR >1 suggests an increase in the radiation dose. For example, an OR of 1.5 signifies a 50% increase in the radiation dose. Additionally, for larger continuous variables, step sizes were increased for angulation and rotation (1 step equaled 30° C-arm angulation or rotation), field size (1 step equaled a 200-cm² decrease), and air gap (1 step equaled a 5-cm decrease). See Supplemental Table S1 (supplementary material available at http://journals. sagepub.com/doi/suppl/10.1177/1526602817697188) for specific calculations. All statistical analyses were performed using R software (version 2.15.1; R Foundation for Statistical Computing, Vienna, Austria; http://www.r-project. org) with lme4 packages (version 1.1–8; Bates, Maechler, and Bolker, 2012).

Prediction Model

The effect estimates derived from regression of the predicted outcomes of DR_{AK} for each combination of a predictor's analysis were used to create a color-coded risk chart showing the maximum allowed radiation duration until the cumulative threshold of 2 Gy would be reached. Additionally, the colors of the risk chart correspond with the X-ray DRs under the varying radiation predictor levels, where dark green represents the lowest dose rate output,
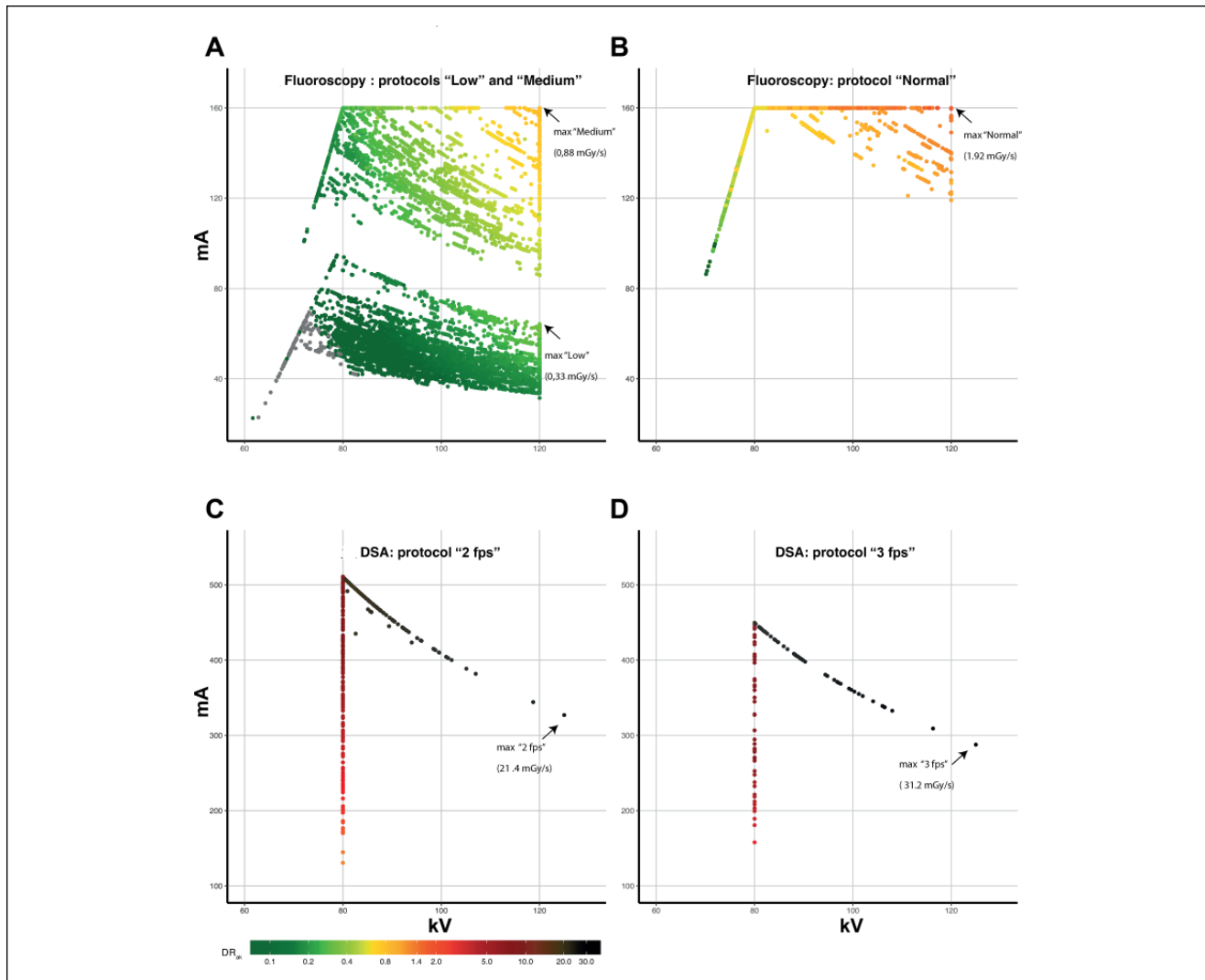
Figure 1. Scatterplots of all fluoroscopy and digital subtraction angiography (DSA) X-ray runs plotted by the peak kilovolt and milliampere setting, showing maximum radiation dose rates for air kerma (DR_{AK}) in mGy/s. (A) DR_{AK} for fluoroscopy protocols "low" and "medium," both corresponding with a 0.4-mm copper filter. (B) DR_{AK} for fluoroscopy protocol "normal," corresponding with a 0.1-mm copper filter. (C) DR_{AK} for DSA using a 2-fps protocol and (D) a 3-fps protocol (both using a 0.1-mm copper filter). Fps, frames per second.

while black corresponds to the highest radiation DRs. A similar chart was constructed for DR_{DAP} at the 500-Gycm^2 threshold.

Results

Of the 18,811 X-ray runs performed in the 74-patient cohort, 1922 were excluded owing to acquisition in a non-abdomen protocol setting (n=786), brief duration (<0.5 seconds; n=731), single-shot runs (n=386), protocol unidentifiable from the mA/kV pattern (n=16), and DSA runs acquired at a 1-fps protocol (n=3). The final analysis of 16,889 X-ray runs consisted of 16,031 (94.9%) fluoroscopy

runs, with a mean DR_{AK} of 0.35±0.31 mGy/s and a mean DR_{DAP} of 74±67 mGycm^2/s, and 858 (5.1%) DSA runs (DR_{AK} 6.8±5.5 mGy/s and DR_{DAP} 1392±1071 mGycm^2/s).

Radiation Protocol

The numbers of X-ray runs acquired in the low, medium, and normal fluoroscopy protocols were, respectively, 8763 (51.9%), 4523 (26.8%), and 2745 (16.3%). The numbers of X-ray runs acquired in the DSA 2-fps and 3-fps protocols were 599 (3.5%) and 259 (1.5%), respectively. Figure 1 shows the distribution of the calculated DR_{AK} per protocol in relation to the kV and mA resulting from fluoroscopy and

Table 3. Mean Radiation Dose Rates (DR) for Air Kerma (DR$_{AK}$) and Dose Area Product (DR$_{DAP}$) per Exposure for Fluoroscopy and Digital Subtraction Angiography (DSA) Protocols.[a]

	Number of Runs	DR$_{AK}$, mGy/s	Time to 2-Gy Skin Threshold, min	Mean DR$_{DAP}$, mGycm^2/s	Time to 500-Gycm^2 Threshold, min	Runs at 120 kV and Maximum mAs, %
Fluoroscopy						
Total	16,031 (94.9)	0.35±0.31	95.9 (106)	74±67	112 (124)	
Low	8763 (51.9)	0.15±0.06 (max 0.33)	217.6 (2015.9–98.5)	41±17 (max 109)	206 (2973–76)	2.3
Medium	4523 (26.8)	0.42±0.18 (max 0.88)	78.8 (403.1–39.7)	76±43 (max 269)	109 (966–31)	5.8
Normal	2745 (16.3)	0.84±0.36 (max 2.0)	39.5 (450.9–17.3)	178±90 (max 629)	47 (436–13)	6.0
DSA						
Total	858 (5.1)	6.79±5.5	4.9 (6.0)	1392±1071	6.0 (7.8)	
2 fps	599 (3.5)	5.71±4.23 (max 21.4)	5.8 (51.2–1.6)	1157±809 (max 6405)	7.2 (40–1.3)	0.23
3 fps	259 (1.5)	9.3±7.07 (max 31.2)	3.6 (28.5–1.1)	1935±1367 (max 6840)	4.3 (49–1.2)	0.12

Abbreviation: fps, frames per second; max, maximum.
[a]Continuous data are presented as the means ± standard deviation or (minimum–maximum); categorical data are given as the counts (percentage).

DSA X-ray runs. Table 3 presents the mean DRs stratified per protocol. The low, normal, and medium fluoroscopy protocols corresponded with means of 218, 79, and 40 minutes, respectively, until the 2-Gy threshold was reached. For DSA imaging, the 2-fps and 3-fps protocols produced means of 5.8 and 3.6 minutes, respectively, until this threshold was reached.

When the mean DRs for fluoroscopy and DSA were compared, DR$_{AK}$ overall increased 19 times. However, when these outcomes were compared per protocol, changing from fluoroscopy low to DSA 2 fps, fluoroscopy medium to DSA 2 fps, and fluoroscopy normal to DSA 2 fps, the DR$_{AK}$ increased approximately 36±11, 15±4, and 7±2 times, respectively. Changing from fluoroscopy low to DSA 3 fps, medium to DSA 3 fps, and normal to DSA 3 fps increased the dose 59±23, 24±8, and 12±3 times, respectively.

C-arm Rotation

For the X-ray runs that were acquired between −15° and 15° of rotation (65.5% of total X-ray runs), the mean DR$_{AK}$ for fluoroscopy was 0.25±0.2 mGy/s and the mean for DSA was 4.2±3.0 mGy/s. The mean DRs increased approximately 3 to 4 times when the C-arm was rotated over 75° to 90°, which was the case in 1073 X-ray runs (6.3%). In this lateral projection, the mean DR$_{AK}$ was 0.75±0.4 mGy/s for fluoroscopy and 14.6±5.6 mGy/s for DSA. See Supplemental Table S2 (DR$_{AK}$ and DR$_{DAP}$ stratified between fluoroscopy and DSA protocols), Supplemental Table S3 (DR$_{AK}$ stratified between fluoroscopy and DSA protocols), and Supplemental Table S4 (DR$_{DAP}$ stratified between fluoroscopy and DSA protocols) (supplementary material available at http://journals.sagepub.com/doi/suppl/10.1177/1526602817697188).

Body Mass Index

The mean BMI was 26.3±3.7 kg/m^2, while the mean body thicknesses were 27.2±2.7 cm for AP and 34.2±2.9 for the lateral measurement. Correlations between BMI and body thickness were 0.83 (r^2=0.36, p<0.01) for AP and 0.66 (r^2=0.24, p<0.01) for lateral as measured at the level of the renal arteries. The mean DR$_{AK}$ increased an average of 9 times for fluoroscopic imaging, from 0.09±0.05 to 0.83±0.5 mGy/s, while DR$_{AK}$ for DSA increased from 1.34±0.5 to 12.5±5.5 mGy/s when the lowest BMI group (<20 kg/m^2) was compared with the highest BMI group (>35 kg/m^2).

Field Size and Source-to-Image Distance

The mean DR$_{AK}$ for the maximum field size (without any collimation or magnification) was 0.13±0.12 mGy/s for fluoroscopy and 1.5±0.8 mGy/s for DSA imaging. Reducing the field size from <1200 cm^2 to >200 cm^2 increased the fluoroscopy DR$_{AK}$ to a mean of 0.63±0.38 mGy/s and increased DSA DR$_{AK}$ to an average of 12.4±5.6 mGy/s. In general, field size showed an opposite effect on DR$_{AK}$ compared with DR$_{DAP}$. Where DR$_{DAP}$ reduces with decreased field size, the DR$_{AK}$ increases when the field size is decreased (Figure 2).

Reducing the air gap by decreasing the source-to-image distance (SID) decreased the mean DR$_{AK}$ for DSA imaging from 11.65±5.1 mGy/s for a 115- to 120-cm SID to a mean DR$_{AK}$ 3.6±3 mGy/s for a SID of 90 to 100 cm.

Univariate Model

All radiation predictors were significant in both the fluoroscopy and DSA protocols as well as the DAP and AK dose simple
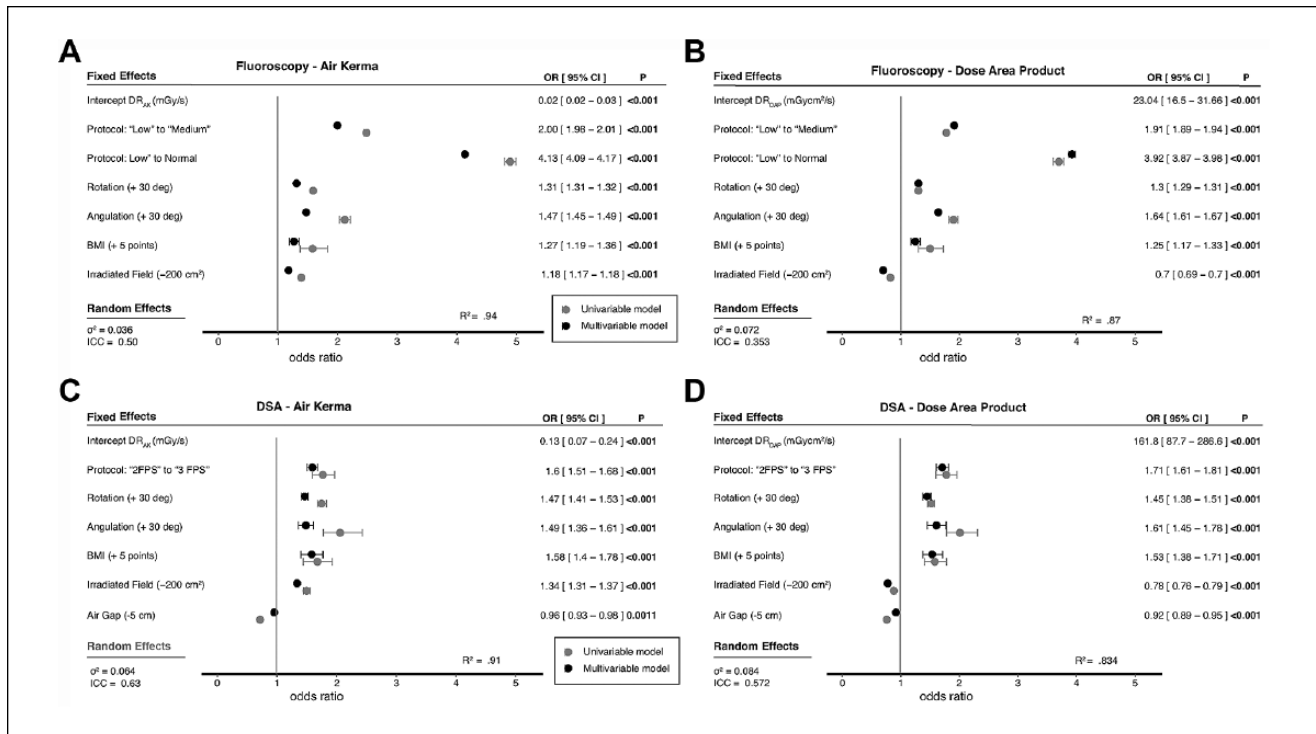
Figure 2. Outcomes of univariate (gray) and multivariate (black) log-linear models for radiation dose rates for air kerma (DR$_{AK}$) in mGy/s and DR$_{DAP}$ in mGycm^2/s for (A, B) fluoroscopy and (C, D) digital subtraction angiography (DSA). R^2 is the overall fit of the model. The fixed and random effects are the outcomes of the multivariate models. BMI, body mass index; OR, odds ratio; CI, confidence interval; ICC, intraclass correlation coefficient.

linear regression models, which can be found in Supplemental Table S5 (supplementary material available at http://journals.sagepub.com/doi/suppl/10.1177/1526602817697188) and are plotted in Figure 2. The largest R^2 (0.81) for DR$_{AK}$ was for the fluoroscopy radiation protocol, while for DSA, C-arm rotation was correlated with the highest R^2 (0.75) for DR$_{AK}$.

Multivariate Model

Significant positive predictors of higher DR in the fluoroscopy DR$_{AK}$ multivariate mixed model were fluoroscopy protocol, C-arm angulation, C-arm rotation, and BMI. Field size was a significant negative predictor. For fluoroscopy, the chosen protocol was the most substantial predictor of DR. For instance, changing from low to medium increased DR$_{AK}$ by 200% and changing from low to normal increased DR$_{AK}$ by 413%. Secondary but also significant predictors of increased DR$_{AK}$ were BMI, C-arm rotation, C-arm angulation, and field size. For example, DR$_{AK}$ increased 27% with a 5-point increase in BMI, 31% for every 30° C-arm rotation, and 47% for every 30° C-arm angulation. With every 200 cm^2 decrease in field size, DR$_{AK}$ increased by 18%. Comparable outcomes were found for DR$_{DAP}$, except for field size. DR$_{DAP}$ decreased by 30% with every decrease of 200 cm^2 in field size.

In the mixed multivariate DSA DR models, the protocol, rotation, angulation, BMI, and field size were significant predictors of higher DR$_{AK}$, whereas SID was a significant negative predictor. Changing the DSA protocol from 2 to 3 fps corresponded with a 60% increase in DR$_{AK}$. A 5-point increase in BMI corresponded with a 58% increase in DR$_{AK}$, an additional 30° of rotation toward 90° increased DR$_{AK}$ 47%, and every 30° of angulation toward 35° increased DR$_{AK}$ 49% (Figure 2). Primary discrepancy in ORs between DR$_{AK}$ and DR$_{DAP}$ were found for field size. With every 200-cm^2 decrease in field size toward 0, DR$_{AK}$ increased 34%, while DR$_{DAP}$ decreased 22%.

Instant Patient Risk Charts

The predicted AK and DAP DRs are shown in a risk chart (Figure 3) displaying various combinations of radiation predictors. The numbers on the chart correspond to the intensity of the radiation dose exposure and the colors indicate the amount of radiation time until dose thresholds are reached. For example, a BMI of 30 kg/m^2 combined with 45° of rotation and a field size of 800 cm^2 in the medium fluoroscopy protocol predicts a DR$_{AK}$ of 0.39 mGy/s (or 85.5 minutes until the 2-Gy skin threshold is reached) and a DR$_{DAP}$ of 0.11 Gycm^2/s (or 75.8 minutes until the 500-Gycm^2 threshold is reached). Maintaining the same settings
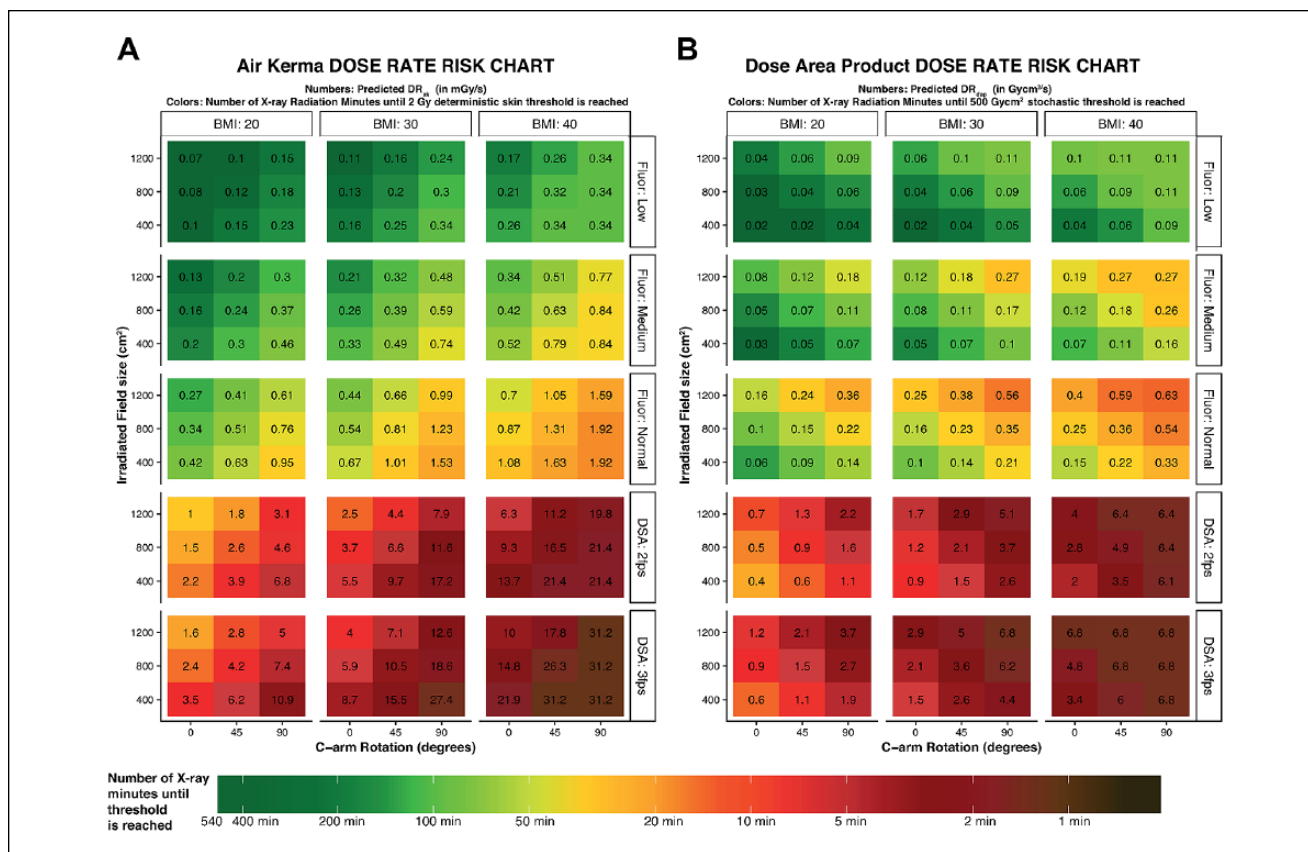
Figure 3. Risk charts for radiation dose rates for (A) air kerma (DR$_{AK}$) and (B) dose area product (DR$_{DAP}$) for fluoroscopy (Fluor) and digital subtraction angiography (DSA) imaging protocols. The color-coding represents the predicted amount of radiation minutes that can be acquired until the 2-Gy skin threshold for DR$_{AK}$ or the 500-Gycm^2 threshold for DR$_{DAP}$ is reached. The gradated color coding system is similar to that used in Figure 1. The numbers in each square correspond with the actual predicted DR (in mGy/s for DR$_{AK}$ and in mGycm^2/s for DR$_{DAP}$). Outcomes were manually refined if the model overestimated the predicted DR vs maximum threshold dose. For all predicted outcomes, the C-arm angulation was set at 0°, and the source-to-image distance was set at 100 cm for the DSA charts. Each risk chart can be used by selecting the body mass index (BMI in kg/m^2) of the patient. The second step is to choose the protocol for the acquisition. For fluoroscopy imaging, 3 protocols are available (low, medium, normal), while 2 fps or 3 fps can be chosen for DSA imaging. Third, the field size (1200 vs 800 vs 400 cm^2) is on the y-axis and the C-arm rotation on the x-axis.

and switching the acquisition to a DSA run with a 2-fps protocol results in a predicted DR$_{AK}$ of 6.6 mGy/s (or 5.0 minutes until 2 Gy) and a predicted DR$_{DAP}$ of 2.1 Gycm^2/s (which equals 4.0 minutes of DSA using these settings until the 500-Gycm^2 threshold is reached).

Discussion

The proposed patient risk chart facilitates instant estimation of radiation risks during the intervention, visualizing the short-term determinant risks and the long-term indirect stochastic radiation risks. The chart demonstrates that intraoperative DRs are highly dependent on not one but a combination of factors: the X-ray mode (fluoroscopy or DSA) with the chosen protocol, the C-arm rotation or angulation, patient BMI, field size, and the SID. Moreover, the effects size differs between the radiation prediction factors and also between DSA and fluoroscopy acquisition.

The X-ray protocol setting of the equipment, mostly predefined by the C-arm manufacturers, plays a key role in determining the C-arm DR. Each protocol has a predefined X-ray radiation maximum, identified by a maximum amount of mA (protocol dependent) and a predefined filter thickness of between 0.4 and 0.1 mm. In addition, the kV is allowed to vary between 80 kV and a maximum of 120 kV, which is protocol independent and also depends on the mA.

The protocol maximums (at maximum kV and mA) are much more often reached in fluoroscopy (20% of all the runs) than in DSA, where reaching the maximum threshold is quite rare (0.3% of the total runs). Therefore, the fluoroscopy image quality might not always be optimal when the protocol's maximum is reached, whereas the DRs with DSA imaging can vary more freely, and the optimum image quality is nearly always achieved. Fluoroscopy maximum doses are limited by the protocols but can be manually changed by the operator. During DSA acquisition, however, the image

quality is not always ideal because the maximum DR is mostly not reached; consequently, the DRs during DSA imaging are also much harder for the operator to control, with the main risk that extremely high DRs are produced.

Unfortunately, these protocol maximum settings are also the main limitation of the current risk charts because the exact maximums per protocol could not be taken into account in the risk charts. Upgrading to a higher fluoroscopy protocol highly affects the intraoperative dose during fluoroscopy and should be kept only for those cases in which the image quality is not sufficient for the task.

Previous studies have mostly focused on measurement of the cumulative total radiation dose per intervention to identify predictors of higher DRs.[6,7] The correlation between DSA runs in fixed C-arms and higher radiation doses compared with fluoroscopy imaging, especially in fixed C-arms, has been studied.[6] In addition, there are concerns about the higher radiation dose exposure during lateral C-arm angulation.[8] BMI >25 kg/m^2 has also been identified as a predictor for higher cumulative radiation doses.[9] However, these studies focused on a single outcome parameter by analyzing the cumulative DRs per intervention and did not account for the multifactorial effect of all of the radiation predictors or correct for the chosen protocols, field size, or air gap for DAP and AK.[9] Because these predictors vary within and between procedures, DRs are also constantly adapted to each status, resulting in varying cumulative radiation doses. Additional DR-specific studies were performed to calculate the effect of rotation using a phantom[4,10] or cadaveric setup,[11] where outcomes limited to a single phantom model are in an experimental setting and are not related to varying body thickness or field size, as in the current study.

Both the AK and DAP models were included to show the reliability of the model as well as the differences between both radiation parameters. In addition, it was assumed that changing from the low to the medium fluoroscopy radiation protocol would double the DR, so the second upgrade from medium to normal should do likewise and double the dose rate. The multivariate model bore this out: the fluoroscopy ORs of 2.0 for the low to medium doubled to 4.13 for the low to normal fluoroscopy protocol. It can therefore be assumed that our outcomes represent a reliable model for the current predictors with the current protocol settings.

The main limitations of the current models are the missing outcome values for SID within the fluoroscopically runs and the exact magnification factors within all runs. Although DR$_{DAP}$ lowers with reduced field size, the DR$_{AK}$ increases with increased field size, causing different effects based on magnification vs collimation. Magnification and collimation both influence the field size but affect the DR changes differently. The field size reduces during collimation, but the exposed dose per cm^2 remains similar; thus, DR$_{DAP}$ will be reduced during collimation, whereas DR$_{AK}$ remains

similar. During magnification, however, the field size and the DRs are both changed. While field size is reduced, the DR is increased, and thus magnification affects both DR$_{DAP}$ and DR$_{AK}$.[12] The exact effect of magnification vs collimation could not be included in the models because these values were not available. However, the effect of magnification appeared mostly in the DR$_{AK}$ model, where it was shown that measurement of AK is independent of field size and the DR$_{AK}$ increases with reduced field size, which can be explained only by using several magnification levels.

In addition, both DR$_{AK}$ and DR$_{DAP}$ were included because DAP and AK represent different effects of radiation (deterministic vs stochastic). Although the DR$_{AK}$ is the most reliable and is independent of the collimation for DR analysis, DAP better correlates with the operator radiation dose and the total absorbed by the patients.[13]

The data used in the current models were acquired using a state-of-the-art fixed imaging machine updated with AlluraClarity, the latest generation of dose-reduction technology. An update with Clarity was shown to be an effective method of reducing the DSA exposure doses[14] even in EVAR.[15] However, the exposure with DSA is still 19-fold larger compared with fluoroscopy, and in extreme cases, up to a factor of 60 when low-dose fluoroscopy is compared with 3-fps high-dose DSA. Overall, the DSA doses using fixed C-arms (independent of this update) are much higher when fixed X-ray equipment is used compared with mobile equipment.[16] Thus, although the latest technologies have been evaluated here, focus on radiation awareness and additional strategies to minimize exposure and occupational risk are relevant.[16]

In our study, only the X-ray runs acquired in the abdomen protocol were included, exclusively for EVAR interventions. The abdominal region in most patients is an area with a large amount of tissue that must be penetrated by X-rays to acquire an image, and the thickness of the tissue influences the amount of radiation required to achieve the optimal image resolution. Most of the X-ray runs required for (complex) EVAR interventions are acquired in the abdominal region. Because complex EVAR interventions performed using fixed C-arms are associated with high DRs, a mean DR$_{DAP}$ >500 Gycm^2 or with a fluoroscopy time >80 minutes are not uncommon.[17]

Finally, all our fluoroscopy runs were acquired at a 15-fps setting. For EVAR interventions, the frame rate for fluoroscopy can vary between 7.5 and 15 fps.[18] Although a 7.5 fps will reduce the intraoperative doses, it may also influence device smoothness. A lower fps rate interferes with the smoothness of a moving object, such as a guidewire, and a fps rate that is too low can hinder the radiologist's eye-hand coordination.[19]

Our outcomes represent the direct DRs as measured by the equipment, without recalculating doses to direct stochastic risks in Sieverts (for DR$_{DAP}$) or the actual peak skin

doses rates (for DR$_{AK}$). Thus, the current DRs were not corrected for tissue radiosensitivity, age, or sex and do not represent the actual stochastic parameter Sieverts, and both DAP and AK are direct outputs and do not include the backscatter factor.[13] However, understanding the multifactorial effect of different radiation predictors on the direct measured DR can provide an insight as to how the final cumulative radiation dose for each patient and C-arm configuration is created.

Analyzing the dose rates in the future will provide better insight into the parameters responsible for the intraoperative exposed radiation doses. Being aware of the major differences between these 2 dose modes is the first step in dose awareness and management, preprocedure planning, procedure simulation, monitoring the real-time radiation dose by the operators,[20] education in radiation management, and familiarization with the imaging protocols and operating modes.[21] We are all aware of the burden of radiation exposure, but good imaging remains a cornerstone for safe and successful endovascular procedures. It remains the responsibility of the primary operator to balance out the minimum exposed radiation dose to obtain maximum outputs, without taking risks of reducing X-ray dose or replacing X-ray runs if this is accompanied by additional patient risks. Optionally, one can consider using 3D CT image fusion to reduce the number of DSA runs, especially in complex fenestrated and branched EVAR.[22,23]

Although not described in this study, intraoperative staff dose rates depend on patient radiation exposure, as well as personal shielding and distance from the X-ray source.[24,25] However, discrepancies may exist between the patient's radiation dose ORs and the operators ORs for each predictor. To understand differences in ORs of the patient and surgeon during EVAR, one first needs to understand the effects on the radiation dose as described in this study. Therefore, the goal of the second part of this study is to combine the patient's radiation dose with the operator's shielding techniques and staff measurements to extract an operator's dose rate prediction model.

Conclusion

For fluoroscopy imaging, the protocol used, BMI, and C-arm rotation were associated with higher radiation doses. In DSA imaging, C-arm rotation, field size, air gap, and BMI were related to higher radiation doses. The choice of protocol was less important in DSA imaging. Risk charts were constructed to help operators understand intraoperative DRs and consequently reduce radiation exposure during EVAR procedures in the hybrid operating suite. One can and should reduce the number DSA runs necessary to a minimum, as well as the amount of time and total frames per second during DSA runs.

References

1. McNally MM, Scali ST, Feezor RJ, et al. Three-dimensional fusion computed tomography decreases radiation exposure, procedure time, and contrast use during fenestrated endovascular aortic repair. *J Vasc Surg*. 2015;61:309–316.
2. Varu VN, Greenberg JI, Lee JT. Improved efficiency and safety for EVAR with utilization of a hybrid room. *Eur J Vasc Endovasc Surg*. 2013;46:675–679.
3. de Ruiter QM, Moll FL, Gijsberts CM, et al. AlluraClarity radiation dose-reduction technology in the hybrid operating room during endovascular aneurysm repair. *J Endovasc Ther*. 2016;23:130–138.
4. Haqqani OP, Agarwal PK, Halin NM, et al. Defining the radiation "scatter cloud" in the interventional suite. *J Vasc Surg*. 2013;58:1339–1345.
5. Monastiriotis S, Comito M, Labropoulos N. Radiation exposure in endovascular repair of abdominal and thoracic aortic aneurysms. *J Vasc Surg*. 2015;62:753–761.
6. Patel AP, Gallacher D, Dourado R, et al. Occupational radiation exposure during endovascular aortic procedures. *Eur J Vasc Endovasc Surg*. 2013;46:424–430.
7. Agarwal S, Parashar A, Bajaj NS, et al. Relationship of beam angulation and radiation exposure in the cardiac catheterization laboratory. *JACC Cardiovasc Interv*. 2014;7:558–566.
8. Albayati MA, Kelly S, Gallagher D, et al. Editor's choice—Angulation of the C-arm during complex endovascular aortic procedures increases radiation exposure to the head. *Eur J Vasc Endovasc Surg*. 2015;49:396–402.
9. Majewska N, Stanisic MG, Klos MA, et al. Patients' radiation doses during thoracic stent-graft implantation: the problem of long-lasting procedures. *Ann Thorac Surg*. 2012;93:465–472.
10. Lee K, Lee KM, Park MS, et al. Measurements of surgeons' exposure to ionizing radiation dose during intraoperative use of C-arm fluoroscopy. *Spine (Phila Pa 1976)*. 2012;37:1240–1244.
11. Haqqani OP, Agarwal PK, Halin NM, et al. Minimizing radiation exposure to the vascular surgeon. *J Vasc Surg*. 2012;55:799–805.
12. Weinberg BD, Guild JB, Arbique GM, et al. Understanding and using fluoroscopic dose display information. *Curr Probl Diagn Radiol*. 2015;44:38–46.
13. Sailer AM, Schurink GW, Bol ME, et al. Occupational radiation exposure during endovascular aortic repair. *Cardiovasc Intervent Radiol*. 2015;38:827–832.
14. van Strijen MJ, Grunhagen T, Mauti M, et al. Evaluation of a noise reduction imaging technology in iliac digital subtraction angiography: noninferior clinical image quality with lower

patient and scatter dose. *J Vasc Interv Radiol*. 2015;26:642–650.e1.

15. van den Haak RF, Hamans BC, Zuurmond K, et al. Significant radiation dose reduction in the hybrid operating room using a novel X-ray imaging technology. *Eur J Vasc Endovasc Surg*. 2015;50:480–486.

16. Kendrick DE, Miller CP, Moorehead PA, et al. Comparative occupational radiation exposure between fixed and mobile imaging systems. *J Vasc Surg*. 2016;63:190–197.

17. Tacher V, Lin M, Desgranges P, et al. Image guidance for endovascular repair of complex aortic aneurysms: comparison of two-dimensional and three-dimensional angiography and image fusion. *J Vasc Interv Radiol*. 2013;24:1698–1706.

18. Akkus NI, Mina GS, Abdulbaki A, et al. Using 7.5 frames per second reduces radiation exposure in lower extremity peripheral vascular interventions. *Vascular*. 2015;23:240–244.

19. Balter S. Fluoroscopic frame rates: not only dose. *AJR Am J Roentgenol*. 2014;203:W234–W236.

20. Baumann F, Katzen BT, Carelsen B, et al. The effect of realtime monitoring on dose exposure to staff within an interventional radiology setting. *Cardiovasc Intervent Radiol*. 2015;38:1105–1111.

21. Bartal G, Vano E, Paulo G, et al. Management of patient and staff radiation dose in interventional radiology: current concepts. *Cardiovasc Intervent Radiol*. 2014;37:289–298.

22. Dias NV, Billberg H, Sonesson B, et al. The effects of combining fusion imaging, low-frequency pulsed fluoroscopy, and low-concentration contrast agent during endovascular aneurysm repair. *J Vasc Surg*. 2016;63:1147–1155.

23. Sailer AM, de Haan MW, Peppelenbosch AG, et al. CTA with fluoroscopy image fusion guidance in endovascular complex aortic aneurysm repair. *Eur J Vasc Endovasc Surg*. 2014;47:349–356.

24. Attigah N, Oikonomou K, Hinz U, et al. Radiation exposure to eye lens and operator hands during endovascular procedures in hybrid operating rooms. *J Vasc Surg*. 2016;63:198–203.

25. Mohapatra A, Greenberg RK, Mastracci TM, et al. Radiation exposure to operating room personnel and patients during endovascular procedures. *J Vasc Surg*. 2013;58:702–709.